

BACKGROUND-INDUCED MEASUREMENT ERRORS OF THE CORONAL INTENSITY, DENSITY, VELOCITY, AND MAGNETIC FIELD

M. J. PENN¹, H. LIN², S. TOMCZYK³, D. ELMORE³ and P. JUDGE³

¹*National Solar Observatory*, 950 N Cherry Av, Tucson AZ 85719, U.S.A.*

²*Institute for Astronomy, University of Hawaii, 2680 Woodlawn Drive,
Honolulu, HI 96822-1897, U.S.A.*

³*High Altitude Observatory, National Center for Atmospheric Research**, P.O. Box 3000,
Boulder, CO 80307, U.S.A.*

(Received 26 January 2004; accepted 31 March 2004)

Abstract. The effect of a background signal on the signal-to-noise ratio is discussed, with particular application to ground-based observations of emission lines in the solar corona with the proposed Advanced Technology Solar Telescope. The concepts of effective coronal aperture and effective coronal integration time are introduced. Specific expressions are developed for the 1σ measurement errors for coronal intensity, coronal electron density, coronal velocity, and coronal magnetic field measurements using emission lines and including a background.

1. Introduction

The ability to make routine seeing-limited high-flux coronal observations would be a new and exciting prospect for the study of solar physics in the corona. The Advanced Technology Solar Telescope (ATST) is a proposed 4-m all-reflecting solar telescope. The current design uses a primary mirror with low scatter and aggressive dust control so that the ATST is capable of observing the solar corona at near-infrared wavelengths with a low background.

Some theories have predicted, and observations at both radio and optical wavelengths have suggested, that coronal structures exist at the 0.1 arc sec (100 km) size scale. Eclipse observations using the 3.6 m Canada-France-Hawaii (CFH) telescope in 1991 successfully observed the evolution of one such feature during 210 s of eclipse totality. Spacecraft observations show structure at the limit of their resolution (down to about 1 arc sec) and show that these structures are numerous and long-lived. The ability of ATST to observe the corona at high spatial resolution will open a new window to observe these structures and to address fundamental questions concerning the heating of the corona and the source of the solar wind.

*Operated by the Association of Universities for Research in Astronomy, Inc. (AURA), under co-operative agreement with the National Science Foundation.

**The National Center for Atmospheric Research is sponsored by the National Science Foundation.



The ATST Coronal Working Group was formed to examine the scientific case for seeing-limited coronal observations, as well as lower-resolution spectroscopic and spectropolarimetric coronal observations. The following information represents some of the work done by this group; for more details please visit the ATST home page on the World Wide Web, <http://atst.nso.edu>.

1.1. THE SCIENTIFIC CASE FOR HIGH-RESOLUTION CORONAL OBSERVATIONS

Theoretical expectations are that there is structure down to 0.1 arc sec and turbulent structure down to less than 1 km (1 milli-arc sec) in the solar corona (Mullan, 1990). These structures may change rapidly, as nanoflares proposed by Parker (1988) might be on the order of 100–1000 km and might last for as little as 1–2 s. Nanoflares may represent not only an energy release site but may also provide momentum to coronal ‘plasmoids’ with initial sizes of 250 km (Mullan, 1990).

Radio observations have implied small-scale coronal structures for a long time. Melrose (1975) showed that meter-wave observations of various solar storm events could only be understood if coronal inhomogeneities existed at the 100 km size scale. Benz (1986) argued that radio emission spikes of millisecond duration imply emission regions with sizes less than 200 km. Aschwanden and Benz (1988) show that decimetric emission in solar flares is best fit with source region sizes of 50–500 km.

Comparison of EUV line emission and optical continuum observations of the corona by Orrall and Rottman (1986) show that the coronal irregularity factor (the ratio of $\langle N^2 \rangle / \langle N \rangle^2$) was high suggesting unresolved, small-scale density fluctuations in the corona.

A 3.6-m telescope (CFHT) was used to observe the corona during the 1991 eclipse. Seeing limited the resolution to between 0.4 and 0.6 arc sec based on measurements of the lunar limb (Delannée *et al.*, 1998; Zhukov *et al.*, 2000). Structure was seen down to the seeing limit; one ‘plasmoid’ was seen within the field of view with a size of 1500 km but with internal structure at the seeing limit of about 400 km; the average height of the plasmoid during observations of its motion was 90 000 km ($R = 1.13 R_{\odot}$).

TRACE images have 0.5 arc sec pixels and show structures down to this limit extending into the corona up to at least 50 000 km height (Schrijver *et al.*, 1999). Comparing TRACE observations with data from the VAULT sounding rocket with 0.33 arc sec resolution showed that much of the chromospheric structure does correspond with small scale coronal structures (Vourlidas *et al.*, 2001). While TRACE or rocket observations cannot approach the limit of the proposed ATST measurements, they do show that fine-scale structures exist in the corona every day, some with extended lifetimes and some showing rapid time evolution.

1.2. CORONAL MAGNETIC MEASUREMENTS

Currently there are few observations of the solar magnetic field at coronal heights in the optical spectrum. As the dynamics of the corona are controlled by the magnetic field, there is great interest in measuring the field there. The free energy of the magnetic field dominates that of the plasma in the corona, and when released it controls or influences everything from loop heating to flares to coronal mass ejections. However, even recent investigations of the coronal heating problem have used extrapolations of the magnetic field measured in the photosphere (Gudiksen and Nordlund, 2002) to infer conditions in the corona, and in the presence of currents in the corona these extrapolations can be incorrect. Some direct observations of the coronal magnetic field are possible at radio wavelengths, and comparisons between these measurements and extrapolated field strengths show discrepancies (Lee *et al.*, 1999; Brosius *et al.*, 2002). Once one has moved outside of the immediate vicinity of active regions, radio observational techniques cannot currently measure the magnetic field strength at high spatial resolution. Recent work shows that near-IR lines can be used to measure the coronal magnetic field at large distances from active regions (Lin, Penn, and Tomczyk, 2000; Judge *et al.*, 2001). This technique, especially with the a coronal emission line at 3934 nm (Kuhn *et al.*, 1999a; Judge *et al.*, 2002) has great promise to provide a new direct window on the magnetic field in the solar corona and strict constraints on magnetic extrapolation models.

2. Signal-to-Noise in Spectral Line Measurements

The problems encountered in background-limited measurements are becoming more common in astronomy. Many observations with the James Webb Space Telescope are expected to be background-limited, and mirror designs are being explored to maximize detection speed (Stockman, Bely, and Burrows, 1996). Basic measurements in LIDAR and thermal IR detectors deal with background-limited ‘detectivity’ issues, and the new search for close-in stellar companions (brown dwarfs and extra-solar planets) faces background-limited detection problems at very small angular size scales.

Background-limited measurements of the solar corona pose problems of high-intensity contrasts of at least 10^5 where large angle scattering (compared to the telescope resolution) of 10–1000 arc sec plays the key role. Coronal emission line measurements provide access to the critical physical parameters of the coronal plasma: the temperature, density, velocity and magnetic field of the corona can be addressed with emission-line measurements. The typical coronal emission-line is observed atop a continuum background comprised of a scattered photospheric spectrum (from sky, instrumental and *F*-corona scattering) plus a small spectrally featureless continuum signal from scattering off high-temperature electrons in the solar corona itself (the continuum or *K*-corona). In all emission-line measurements

including filter and spectrograph measurements and a variety of background subtraction techniques, the signal-to-noise ratio of the measured spectrum plays the critical role in the ability of the measurement to derive the physical parameters in the corona.

In the following discussion the approximation is made that the main systematic properties of the detector have been removed. Specific assumptions include the following: the read noise, dark currents and noise from the dark currents are very small compared to the coronal intensity, there is no extra measurement error introduced by the gain correction (flat-field) step, and there is no noise introduced by time variation of the atmosphere or the instrument. The measurement noise will be determined by photon noise, which is governed by Poisson statistics so that the noise in an intensity measurement is equal to the square-root of that intensity $\sigma_{I_x} = \sqrt{I_x}$. Standard error propagation is used below, so that the error σ_y in a quantity $y(x)$ is given by the square-root of the partial derivative squared times the measurement error squared.

For background-dominated measurements it is critical to understand how the Poisson noise from the background affects the signal-to-noise ratio in the final background subtracted signal. The total intensity is simply the sum of the coronal and background intensities $I_{\text{tot}} = I_{\text{cor}} + I_{\text{bg}}$. To find the coronal intensity the background is subtracted from the total intensity,

$$I_{\text{cor}} = I_{\text{tot}} - I_{\text{bg}}.$$

The noise in the total intensity is simply expressed as

$$\sigma_{I_{\text{cor}}} = \sqrt{\sigma_{I_{\text{tot}}}^2 + \sigma_{I_{\text{bg}}}^2}.$$

Simply computing the signal-to-noise ratio then

$$I_{\text{cor}}/\sigma_{I_{\text{cor}}} = \sqrt{I_{\text{cor}}} \sqrt{\frac{I_{\text{cor}}}{I_{\text{tot}} + I_{\text{bg}}}}.$$

Since with no background the S/N ratio is simply $I_{\text{cor}}/\sigma_{I_{\text{cor}}} = \sqrt{I_{\text{cor}}}$, the S/N with a background is just the S/N without a background times a fraction $(S/N)_{\text{bg}} = f_{\text{bg}}(S/N)$, where

$$f_{\text{bg}} = \sqrt{\frac{I_{\text{cor}}}{I_{\text{tot}} + I_{\text{bg}}}} = \sqrt{\frac{1}{1 + 2I_{\text{bg}}/I_{\text{cor}}}}.$$

In the limit where the background intensity is measured perfectly, which means that the value of I_{bg} is measured exactly (for example by measuring the continuum in a coronal spectrum an infinite number (of times) the factor of two preceding the background to coronal intensity ratio drops to a value of exactly one (see Equation (4) in Section 4.1) and so the multiplicative fraction f for the change in the signal to noise ratio with perfect background removal is given by

$$f = \sqrt{\frac{1}{1 + I_{bg}/I_{cor}}}. \quad (1)$$

3. Effective Coronal Aperture and Integration Time

The achieved S/N ratio determines the ability of the ATST data to measure the physically interesting parameters in the solar corona: the temperature, density, velocity and magnetic field. Since these parameters are mostly measured by using spectroscopy of emission lines (or spectropolarimetry of those emission lines) the S/N ratio of the coronal spectrum is a fundamentally important parameter. A spectrum with a low signal-to-noise ratio will result in large measurement errors for these physical quantities. In the following discussions the S/N ratio is used as the guiding parameter.

An important concept results from a comparison of the effect of this background term on the coronal S/N with the S/N achieved in background-free conditions by two telescopes of different size. While discussing the S/N ratio achieved with telescopes of different apertures it's useful to note that the measured intensity $I_{cor} = F_{cor}t$ where F_{cor} is the detected flux in photons per second and t is the integration time. For two telescopes with diameters D_1 and D_2 and with integration times t_1 and t_2 the S/N ratio $R_{12} = (S/N)_1/(S/N)_2$ achieved for a given integration time is simply

$$R_{12} = \frac{\sqrt{I_1}}{\sqrt{I_2}} = \frac{\sqrt{F_1 t_1}}{\sqrt{F_2 t_2}} = \frac{D_1 \sqrt{t_1}}{D_2 \sqrt{t_2}},$$

since the detected flux varies as D^2 . For a given coronal source intensity, we can define a background brightness b_1 as $b_1 = I_{bg1}/I_{cor}$. Now two different background conditions can be shown to act on the S/N ratio such that $R_{12} = f_1/f_2$. By setting the exposure times to be equal $t_1 = t_2$ we can define an *effective coronal aperture* D_{eff} with the ratio of the two background conditions as

$$D_{eff} = \left(\frac{f_1}{f_2} \right), \quad D_2 = \sqrt{\frac{1 + b_2}{1 + b_1}} D_2. \quad (2)$$

If the background conditions in case 1 are much brighter than the background conditions in case 2 ($b_1 > b_2$) then the effective coronal aperture will decrease from D_2 to D_{eff} in the manner shown above in terms of the resulting S/N ratio in the measurement.

For the specific case of the proposed 4-m ATST telescope it is instructive to look at the effective coronal aperture in different cases. For a true coronagraph at a good site the measured background level at 1000 nm can be less than 10^{-5} in terms of solar disk center brightness, B_{\odot} (see Table II). The intensity of the 1074.6 nm

TABLE I
Photon fluxes.

	Photons
Integrated disk 1000 nm	$3.75e17 \text{ s}^{-1} \text{ m}^{-2} \text{ \AA}^{-1}$
Disk arc sec^{-2}	$1.29e11 \text{ s}^{-1} \text{ m}^{-2} \text{ \AA}^{-1}$
Atmosphere (0.98)	$1.26e11 \text{ s}^{-1} \text{ m}^{-2} \text{ \AA}^{-1}$
ATST Mirrors (0.90)	$1.13e11 \text{ s}^{-1} \text{ m}^{-2} \text{ \AA}^{-1}$
4-m ATST	$1.42e12 \text{ s}^{-1} \text{ \AA}^{-1}$
Spectrograph (0.01)	$1.42e10 \text{ s}^{-1} \text{ \AA}^{-1}$
2 \AA wide emission line	$2.84e10 \text{ s}^{-1}$
40 millionths intensity	$1.14e06 \text{ s}^{-1}$
Signal/noise (1s)	1.07e03

[Fe XIII] emission line can be $4 \times 10^{-5} B_{\odot}$ at $R = 1.1 R_{\odot}$ (Penn and Kuhn, 1994a) and sometimes brighter. This implies a value of about $b_2 = I_{bg}/I_{cor} = 0.2$ as representative of a telescopic coronagraph at a good site. Figure 1 shows how the coronal aperture of the 4 m ATST varies as the background condition is changed from this case to larger values representative of typical scattered light measured at non-coronal sites and with standard solar telescopes (background of $10^{-3} B_{\odot}$, so $b_1 = 20$).

A similar discussion can be used to investigate the effect of different background conditions on the effective integration time required to achieve a certain S/N ratio for a coronal observation. Now the apertures of the two telescopes are set equal: $D_1 = D_2$. Since the measured intensity varies linearly with the integration time the *effective coronal integration time* t_1 will increase with an increasing ratio of background intensity to coronal emission intensity as

$$t_1 = \left(\frac{f_1}{f_2}\right)^2, \quad t_2 = \frac{1 + b_1}{1 + b_2} t_2. \quad (3)$$

Again a good coronal case is defined as $b_2 = 0.2$ and the normalized exposure time is examined as b_1 varies from coronal to non-coronal. Figure 2 shows the results.

4. Sensitivity to Physical Parameters

Simple emission-line imaging will address some of the basic questions in the corona involving the smallest spatial scales that are visible. Motions of plasmoids and coronal loops in the plane of the sky, and brightness variations in these structures (i.e., nanoflares and oscillations) are the main science topics to be explored with simple imaging techniques.

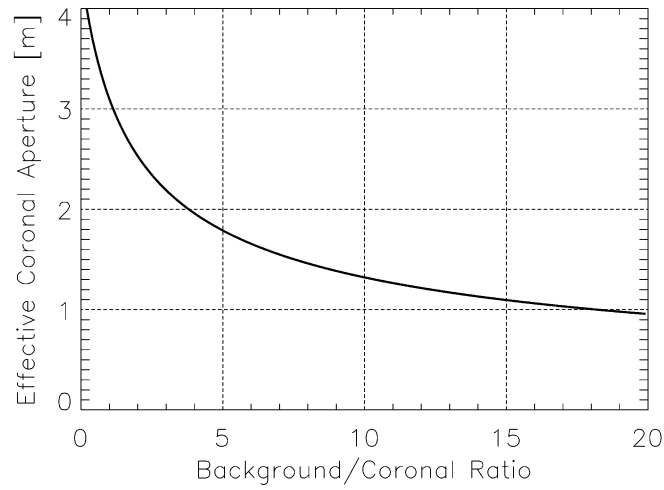


Figure 1. An increasing background introduces photon noise into any coronal measurement even if that background is perfectly removed, thus decreasing the signal-to-noise ratio of the measurement. This reduced signal-to-noise ratio is the same as if the measurement were made with a smaller aperture telescope under lower background conditions. Thus the effective coronal aperture D_{eff} shows how a smaller telescope with a background to coronal ratio of only 0.2 could make the same measurement as ATST under conditions given by the x -axis.

TABLE II
Background measurements NSO/SP JESF.

Date	Wavelength (nm)	Height R_{\odot}	Total background $10^{-6} B_{\odot}$	Line center $10^{-6} B_{\odot}$	Reference
2 May 1993	1074.6 nm	1.11	28	40	Penn, unpub.
2 May 1993	1079.8 nm	1.11	40	15	Penn, unpub.
17 Sep. 1993	1074.6 nm	1.07	40	20	Penn and Kuhn, 1994b
26 Nov. 1993	1074.6 nm	1.10	?	40	Penn and Kuhn, 1994a
14 Oct. 1999	1074.6 nm	1.15	?	14	Lin, Penn, and Tomczyk, 2000
23 Oct. 1999	1074.6 nm	1.12	?	9	Lin, Penn, and Tomczyk, 2000
17 Sep. 1993	1430.0 nm	1.07	8	0	Penn and Kuhn, 1994b
26 Nov. 1993	1430.0 nm	1.10	19	4	Penn and Kuhn, 1994a
26 Nov. 1993	1430.0 nm	2.00	3	0	Penn and Kuhn, 1994a

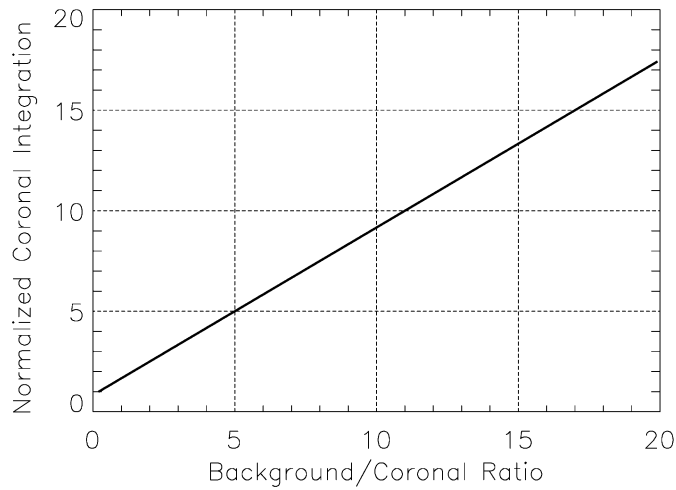


Figure 2. The reduced signal-to-noise ratio in a given measurement by photon noise from a high background can be improved again by integrating for a longer time. This effective coronal exposure plot shows the linear increase in exposure time as the background increases required to obtain the signal-to-noise ratio under conditions of the background to coronal intensity ratio of 0.2.

Line ratio techniques can be used to measure plasma temperature (when different ions are used) or plasma density (when different lines of the same ion are used). The heating mechanism of the corona is still unknown, and temperature changes in dynamic events like flares and ‘coronal rain’ is also a mystery. Plasma density in each of these events, and density and density changes near prominences and during coronal mass ejections are unknown currently.

Line-of-sight motions and magnetic fields can be determined from the centroids of emission lines in spectra and polarized spectra respectively. Plasma velocity in 3-dimensions in coronal loops and during coronal mass ejections are critical science topics. Magnetic field measurements of any kind, from active-region-size scales down to measurements of individual bright loops, during flare and coronal mass ejection events as well as in the quiescent corona will provide critical information about the magnetically controlled coronal plasma.

What is the sensitivity of the ATST to coronal emission? A simple photon flux calculation is listed in Table I for a 2 \AA wide 1074.6 nm emission line. Spatial dispersion of 1 arc sec^2 per pixel and an integration time of 1 s is used. Perfect dark and flat-field correction is assumed, as well as a 100% detector quantum efficiency; however, an instrumental throughput of only 1% is assumed for the spectrograph. No background is involved in this calculation; it is purely based on the measured intensity of the emission line.

The computed signal-to-noise for measuring the wavelength integrated intensity is over 1000. This can then be used to compute the coronal intensity which

represents the 1σ noise level; this intensity is $\sigma_I = (40 \times 10^{-6} B_\odot)/(S/N) = 3.7 \times 10^{-8} B_\odot$ (converting B_\odot to energy units at 1000 nm the noise level is $3.7 \times 10^6 \text{ erg cm}^{-2} \text{ s}^{-1} \text{ sr}^{-1} \text{ \AA}^{-1}$).

The following sections contain a simple look at the background-induced errors for several types of coronal measurements. In each section one parameter with one error is determined for each of the assumed instrument pixels. Complications from other issues, such as the line-of-sight integration effects in the corona, are ignored.

4.1. EMISSION LINE IMAGING: SUBTRACTIVE TECHNIQUE

Imaging to reveal the coronal emission line structures must involve subtracting the background continuum values. As discussed previously the background is dominated by a scattered photospheric spectrum (from the sky, instrument and zodiacal dust) but also should contain a contribution from the K -corona. In general if the background is measured a number of independent times n_{bg} then the background is simply the mean of these measurements $I_{bg} = 1/n_{bg} \sum_{j=1}^{n_{bg}} I_{bg}(j)$. More specifically, if the background is approximated as spectrally constant, the background level is computed as an average of several continuum points where the emission line signal is zero:

$$I_{bg} = \frac{1}{n_{\text{cont}}} \sum_{j=1}^{n_{\text{cont}}} I_{\text{cont}}(j).$$

The error in the computed background level can be expressed as $\sigma_{I_{bg}} = \sqrt{I_{bg}/n_{bg}}$. Including this error in the background determination, the signal-to-noise ratio (S/N) can be more strictly defined as

$$I_{\text{cor}}/\sigma_{I_{\text{cor}}} = \sqrt{I_{\text{cor}}} \frac{\sqrt{I_{\text{cor}}}}{\sqrt{I_{\text{tot}} + \frac{I_{bg}}{n_{bg}}}}.$$

Including this background measurement error in the previous discussion, a new fractional increase in the S/N measurement $(S/N)_{bg} = f'_{bg} \times (S/N)$, where

$$f'_{bg} = \sqrt{\frac{1}{1 + I_{bg}/I_{\text{cor}}(1 + 1/n_{bg})}}. \quad (4)$$

Two cases deserve mention here. When $n_{bg} = 1$, the simplest case of one background and one emission line measurement results in the factor of two coefficients discussed in Section 2, and Equation (1) can now be seen to be defined by

$$f = \lim_{n_{bg} \rightarrow \infty} (f'_{bg}).$$

Rigorous treatment of the number of background measurements effectively multiplies the previous background to coronal intensity parameter b such that $b'_1 = b_1(1+1/n_{bg})$. Since the [Fe XIII] 1074.6 nm emission line has a measured Gaussian line width of about 0.15 nm, a spectral dispersion of about 0.05 nm pixel⁻¹ seems like a reasonable value. A spectral frame with 1024 pixels thus covers 51.2 nm of spectrum. Examining the nearby photospheric spectrum from 1050–1080 nm shows roughly 10 nm of clean continuum giving $n_{bg} = 66$ measurements of the background, and setting $b'_1 = 1.02 b_1$. With so many continuum pixels available at this low spectral dispersion this is only a small increase over the ideal background measurement scenario. With larger spectral dispersion or a smaller spectral field of view fewer background measurements will be made, thus reducing the signal-to-noise ratio.

Using the zero background condition described above, where 1 s integration and 1 arc sec² pixels resulted in a noise level of $\sigma_I = 3.7 \times 10^{-8} B_\odot$, the dependence of the noise level on the background level can be examined. Figure 3 shows a plot using

$$\sigma_{I_{bg}} = \frac{\sigma_I'}{f_{bg}}, \quad (5)$$

with the solid line showing $b'_1 = 1.02 b_1$ as above, and the dashed line using only 2 continuum points with $b'_1 = 1.5 b_1$.

4.2. CORONAL TEMPERATURE AND DENSITIES: LINE-RATIO TECHNIQUE

Coronal temperatures are usually measured using the ratio of line emission from different ions of the same species (Guhathakurta, Fisher, and Altrock, 1993) and coronal electron densities are diagnosed using line ratios from different lines from the same ion of the same species (Penn *et al.*, 1994). Line-ratio techniques employ background subtraction first, and then take a ratio of the spectrally integrated line emission. Measurement error in both of these steps will propagate into measurement error in the resulting ratio and then the physical parameter derived from this ratio.

The line ratio of the two [Fe XIII] lines at 1074.6 nm and 1079.8 nm is used to study the electron density of the emitting plasma. A fit to early work by Flower and Pineau des Forêts (1973) shows that at a height of 1.1 R_\odot the electron density N_e varies roughly as $N_e = 4.121 \times 10^8 q^{-1.67}$ where q is the ratio of emission in the 1074.6 nm line divided by emission in the 1079.8 nm line, $q \equiv I_{75}/I_{80}$. Measurements of the electron density using this line ratio have measured densities commonly accepted for coronal structures, but have shown an unexpected relationship compared to line emission (Penn and Kuhn, 1994a) and recent work (Landi, 2002) has called into question the calculations leading to Fe XIII density diagnostics (and some limitations of this line-ratio technique are discussed by Judge, Hubeny, and Brown, 1997). However, this relationship will be used for illustrative purposes.

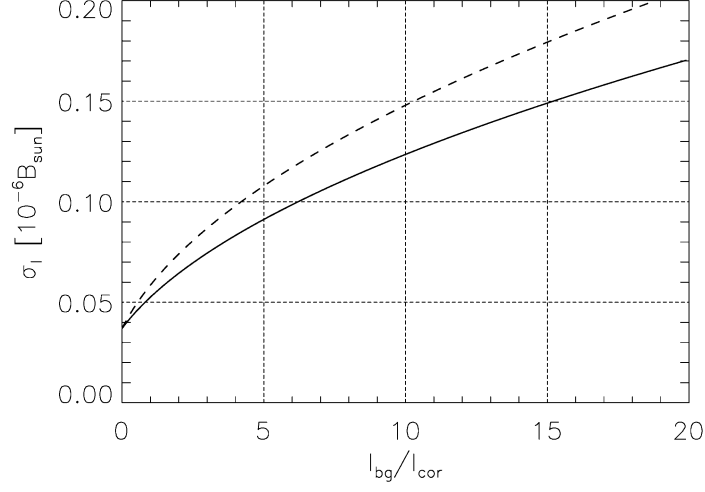


Figure 3. ATST coronal intensity noise (1σ) in units of $10^{-6} B_{\odot}$ (see text) for two background subtracting cases: the *solid line* is for 66 continuum points used to measure the background, and the *dashed line* is for just 2 continuum points used to measure the background. The calculation assumes a coronal brightness of $40 \times 10^{-6} B_{\odot}$ in the 1074.6 nm [Fe XIII] emission line, 1-s integration, and 1 arc sec² spatial pixel size.

Error propagation through this relation shows that the error in the measured electron density σ_{N_e} is related to the error in the line ratio σ_q by $\sigma_{N_e} = 6.88 \times 10^8 q^{-2.67} \sigma_q$. The error in the line ratio can be expressed in terms of the individual intensity measurements $\sigma_{I_{75}}$ and $\sigma_{I_{80}}$ as follows:

$$\sigma_q = (1/I_{80}) \sqrt{\sigma_{I_{75}}^2 + q^2 \sigma_{I_{80}}^2}.$$

Using the line intensities from Penn and Kuhn (1994a) (in units of $10^{-6} B_{\odot}$),

$$q = I_{75}/I_{80} = (40/10) = 4,$$

then the error in the line ratio can be expressed simply in terms of the signal-to-noise ratio of the 1074.6 nm data as $\sigma_q = 4\sqrt{2}(\sigma_{I_{75}}/I_{75})$ and so the error in the electron density measurement can be expressed as

$$\sigma_{N_e} = 3.89 \times 10^9 q^{-2.67} (\sigma_{I_{75}}/I_{75}). \quad (6)$$

With no background this implies an error in the measured line ratio of only $\sigma_q = 5.287 \times 10^{-3}$ and thus an electron density error of only $\sigma_{N_e} = 8.98 \times 10^4 \text{ cm}^{-3}$. Adding a background results in an expression identical to Equation (5). The behavior of the electron density error with increasing background is shown in Figure 4, and is identical in form to the intensity sensitivity of Figure 3.

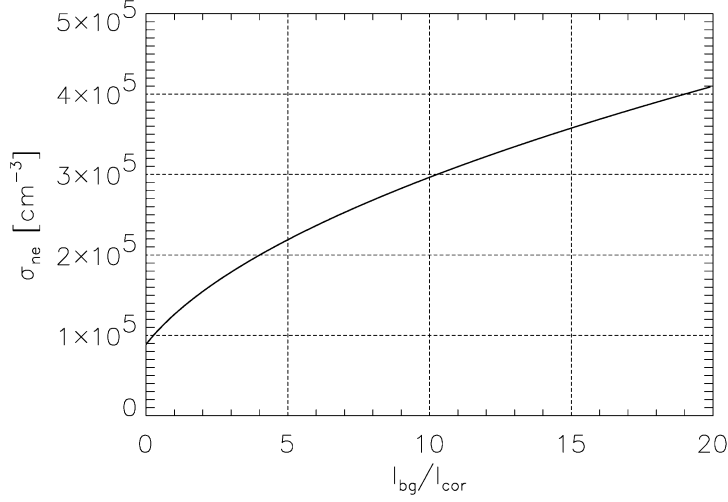


Figure 4. ATST coronal density noise (1σ) in units of electrons cm^{-3} (see text). The calculation assumes a coronal brightness of $40 \times 10^{-6} B_{\odot}$ in the 1074.6 nm [Fe XIII] emission line and the intensity of the 1079.8 nm line is a factor of 4 smaller; 1-arc-sec pixels and 1-s exposures are assumed, with simultaneous measurements in both lines and a with 66 background measurements. The ratio of background to coronal brightness is relative to the 1074.6 nm intensity.

4.3. CORONAL VELOCITY AND MAGNETIC FIELD: LINE CENTROID TECHNIQUE

Computing the plasma velocity via the emission line Doppler shift involves finding the centroid of an emission line which has been background subtracted; finding the magnetic field involves computing the shift difference between the $I + V$ and $I - V$ emission peaks.

If the coronal emission line is approximated as a triangular function, it can be shown that the centroid error is

$$\sigma_v = \frac{cW}{\sqrt{2}\lambda} \frac{\sigma_I}{I_L}, \quad (7)$$

where the centroid error is expressed as a velocity σ_v , W is the width of the line, and σ_I/I_L the reciprocal of the signal to noise of the summed spectral line. Using the 1074.6 nm [Fe XIII] emission line with the signal-to-noise ratio of 1070 computed above, for a 1 arc sec² pixel for a 1-s integration, and using $W = 0.2$ nm, the velocity error is computed to be $\sigma_v = 37$ m s⁻¹.

With polarization measurements the intensity is reduced by a factor of two (in the perfect case) reducing the signal to noise in the spectrum by a factor of $\sqrt{2}$. The magnetic field can be found using a dual beam polarimeter and differencing the computed centers of two emission lines (in the $I + V$ and $I - V$ Stokes spectra); by assuming that each line has the same centroid error, this subtraction introduces

another factor of $\sqrt{2}$ into the calculation. Modifying the expression from McPherson, Lin, and Kuhn (1992) and inserting this extra factor of two the magnetic field error can be computed as

$$\sigma_B = \frac{2\sigma_v}{4.7 \times 10^{-12} c g \lambda} = \frac{\sigma_v}{2.274} = \frac{cW}{3.216\lambda} \frac{\sigma_I}{I_L} \quad (8)$$

(using $g = 1.5$ and $\sigma_v = 37 \text{ m s}^{-1}$ with $\lambda = 1074.6 \text{ nm}$). The error $\sigma_v = 37 \text{ m s}^{-1}$ gives us $\sigma_B = 32.6 \text{ G}$.

Does this number agree with values from current studies using the 40 cm JESF from Lin, Penn, and Tomczyk (2000)? That work used effective integration times of 22 min (1320 s), observed a region of 240 arc sec², but had only 0.01 times the collecting aperture of the proposed 4 m ATST, and observed a region with a brightness of only $14 \times 10^{-6} B_\odot$, resulting in a collection of 1109 times the number of photons and thus an decrease in σ_B by $\sqrt{1109}$ from photon statistics. This implies that the magnetic error should be reduced by a factor of 33.3 resulting in a predicted 1σ error of $\sigma_B = 1 \text{ G}$ for those measurements. The actual 1σ errors are about $\sigma_B = 0.2 \text{ G}$. The background to coronal ratio in the measurements from Lin, Penn, and Tomczyk (2000) is about four, so there is another factor of 2 in the predicted error, resulting in an overall discrepancy of a factor of 10 smaller measured error than that predicted. There may be several sources for this discrepancy, primarily the following: (1) the overall telescope and spectrograph efficiency may be higher than those assumed in Table I (using a 6% spectrograph efficiency rather than 1% reduces the discrepancy to a factor of 2.5) and (2) the absolute intensity of the coronal emission was not measured, rather it was extrapolated with a method which might have a systematic error.

Figure 5 shows the magnetic measurement noise as a function of increasing background; again since the magnetic measurement noise is linearly related to the spectral signal to noise ratio the behavior is identical to those seen in Figure 3 and Figure 4.

Basically each method used here computes the magnetic error as the product of a coefficient from the error propagation c_e and the signal to noise ratio of the observed spectrum $\sigma_B = c_e(\sigma_I/I_L)$. In the method outlined above (centroiding) the coefficient for the 1074.6 nm [Fe XIII] emission line is

$$c_e = \frac{cW}{3.216\lambda} = 1.7 \times 10^4.$$

Another approach is to use the Stokes V profile rather than simply computing the wavelength difference of the centroids of each $I + V$ and $I - V$ emission line. Using the weak field approximation

$$V = \delta\lambda_H \cos \gamma \frac{\partial I}{\partial \lambda}$$

and the magnetic flux is equal to the wavelength integral of the Stokes V profile:

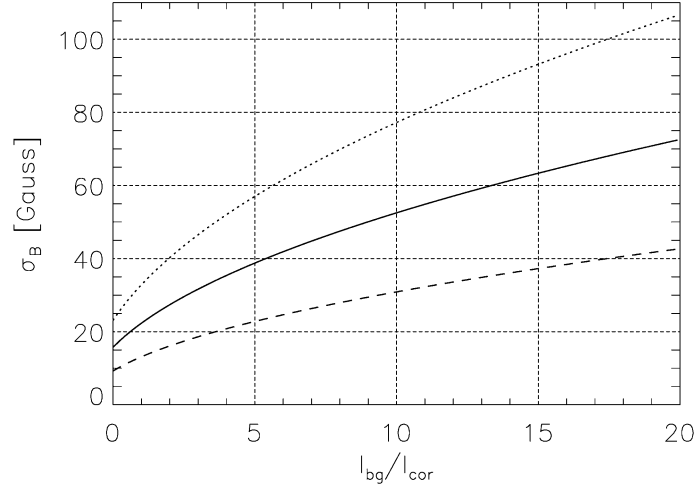


Figure 5. ATST coronal magnetic noise (1σ) in units of gauss (see text). The calculation assumes a coronal brightness of $40 \times 10^{-6} B_{\odot}$ in the 1074.6 nm [Fe XIII] emission line 1-arc-sec pixels and 1-s exposures, and simultaneous measurements in both lines and with 66 background measurements. The *solid line* is from the simple triangular line model, the *dotted line* is from the Harvey rule-of-thumb (virtually identical to using the Stokes V profile integration technique) and the *dashed line* is an extrapolation to 1-s integration from Figure 1 of Kuhn *et al.* (2003).

$$\phi_A = \left| \int_{-\infty}^0 V(\lambda) d\lambda - \int_0^{\infty} V(\lambda) d\lambda \right|.$$

Using a Gaussian emission profile $I(\lambda) = A_0 \exp(-\lambda^2/2\sigma)$ and computing the derivatives and the integrals gives $\phi_A = 2\delta\lambda_H \cos \gamma A_0$. Substituting $\delta\lambda_H = 4.67 \times 10^{-12} g\lambda^2 B$ (where all wavelengths are in nm) and setting $\cos \gamma = 1$, the magnetic error can be computed as

$$\sigma_B^2 = (1/c_2 A_0)^2 \sigma_{\phi_A}^2 + (\phi_A/c_2 A_0^2)^2 \sigma_{A_0}^2,$$

where the value for $c_2 = 4.67 \times 10^{-12} g\lambda^2 = 8.147 \times 10^{-6}$. The error in ϕ_A can be estimated using the number of pixels and the error in the intensity as $\sigma_{\phi_A} = 2\sigma_I/\sqrt{n_{pix}}$. With the same spectral dispersion as in Lin, Penn, and Tomczyk (2000) the number of pixels across the Stokes V profile is roughly 26.

Ignoring the second term of the error expression (it contains the term ϕ_A/A_0 which is very small since B is weak; Lin Penn, and Tomczyk (2000) report a Stokes V amplitude of 4×10^{-4} of the line intensity) and simply approximating the error as $\sigma_B \approx (1/c_2 A_0) \sigma_{\phi_A} = \frac{2}{2\sqrt{n_{pix}} c_2 A_0} \sigma_I$, then the magnetic error is in the form of a constant times the signal to noise in the original spectrum. In this case the constant is (where $n_{pix} = 26$):

$$c_e = \frac{2}{2\sqrt{n_{pix}} 8.147 \times 10^{-6}} = 2.4 \times 10^4.$$

These values agree with the centroid method using the simple rule-of-thumb provided by Harvey (1988) $\sigma_v = (W_{instr} W_{line})^{1/2} \sigma_I / I$ where the instrumental and line widths are in meters per second. In the case discussed here the instrumental width and line width are set equal (since the spectral line is integrated) $(W_{instr} W_{line})^{1/2} \sim W_{line} = 55814 \text{ m s}^{-1}$. This results in an error propagation constant $c_e = 2.5 \times 10^4$; using different instrumental widths requires recomputing the spectral signal to noise as fewer photons are counted in each spectral bin, and the gain from increasing the resolution is balanced by loss of signal to noise in the spectrum.

Although based on different techniques, these three methods yield expressions for the magnetic field error with very similar coefficients, ranging only from 1.7– 2.5×10^4 . A published calculation from Figure 1 of Kuhn *et al.* (2003) (assuming the spatial dispersion is 1 arc sec² and the background contribution is negligible at a height of 1.1 R_\odot) gives a coefficient of $c_e = 10^4$. The only observations which can be used to extrapolate to the ATST are the NSO/SP JESF observations reported by Lin, Penn, and Tomczyk (2000). There the numerical value of the coefficient must be $c_e = 4000$.

5. Sky Properties

The total background which will exist in coronal observations is simply the sum of the sky brightness background and the instrumental scattered light at a given limb height. The ATST Site Survey Instrument will include a Sky Brightness Monitor (SBM). The SBM will measure sky brightness at several wavelengths across the sky from about 4.0 R_\odot to 8.0 R_\odot . The Evans photometer (Evans, 1948) measures the average sky brightness in the region from about 2.0 R_\odot to 5.0 R_\odot but only at the wavelength of the coronal green emission line (530 nm).

In order to extrapolate the SBM or Evans photometer measurements to the predicted ATST coronal field of view and wavelength (roughly 1.1 R_\odot to 2.0 R_\odot at 1000 nm) the radial (and wavelength) variations of the sky must be examined.

5.1. MEASURED SKY BRIGHTNESSES

Sky brightness measurements from NSO/Sac Peak have been made visually at 530 nm since before 1985 and at Haleakala visual sky brightness measurements have been regularly made at the same wavelength since 1987. Kuhn *et al.* (1999b) compare the measurements from the two sites.

Measurements of the sky brightness at 1074.6 nm and 1430 nm were done during the 1990s from Sac Peak using the NSO/JESF 40 cm coronagraph. Results are summarized in Table II. In Table II, the ‘Total background’ refers to the continuum intensity measured with the camera and includes both atmospheric scattering and

instrumental scattering. The ‘Line center’ intensity represents the intensity of only the coronal emission line, after the background has been subtracted.

Eclipse measurements at 1074.6 nm were made from Mauna Kea on 11 July 1991 at $R = 1.12$; the 1074.6 nm emission line intensity was measured at roughly $0.3 \times 10^{-6} B_{\odot}$ and the coronal continuum brightness was measured at $0.1 \times 10^{-6} B_{\odot}$. There may be some scatter and/or absorption from cirrus in these measurements.

5.2. MEASURED RADIAL VARIATIONS

How does sky brightness change with radial height above the limb? The seminal Figure 6 of van de Hulst (1953) shows that a ‘clear sky with haze’ drops from about $10^{-2.67}$ at $1 R_{\odot}$ to about $10^{-4.27}$ at $5 R_{\odot}$ roughly following $1.89 \times 10^{-3} R_{\odot}^{-2.257}$. Measurements from Kuhn *et al.* (2003) show a variation of the sky measured with Solar C roughly following $2.372 \times 10^{-4} R_{\odot}^{-1.778}$. Measurements provided by Elmore from Mauna Loa Solar Observatory show that the background for the MkIV refractive coronagraph follows $11.2 \times 10^{-6} R_{\odot}^{-0.776}$ after cleaning the coronagraph lens, and had the identical radial behavior but with a coefficient of 18.6×10^{-6} before cleaning the lens. Since the exponent did not change, it is likely dominated by atmospheric scattering with a small instrumental component.

5.3. MEASURED WAVELENGTH VARIATIONS

Background intensity changes with wavelength were measured to follow only $\lambda^{-0.6}$ by Penn and Kuhn (1994a) instead of the λ^{-4} behavior expected from pure Rayleigh scattering. These measurements were done using the NSO/JESF 40 cm coronagraph and involve an unknown instrumental contribution.

5.4. TEMPORAL FLUCTUATIONS

If the polarization measurements are done in a sequential way, rapid fluctuations in the sky background will alter some polarization states and not others, leading to systematic errors in the polarization results. This is especially important for very rapid changes such as those caused from forward scattering off of moving particles in the atmospheric optical path.

All Stokes states should be measured simultaneously to remove systematic errors caused by sky fluctuations. An additional slow chopping technique where orthogonal polarization states are swapped on the detectors can be employed to remove systematic effects from detector calibration problems.

6. Summary

There are many reasons to observe the solar corona optically at high spatial resolution. Theory and radio observations suggest that small-scale spatial structures exist, and such structures have been directly observed by high-resolution eclipse and spacecraft measurements. Direct measurements of the coronal magnetic field will provide a new window into the dynamics of coronal heating, flares and coronal mass ejections and will provide strict constraints for testing magnetic field extrapolation techniques. The ability to measure physically important coronal parameters depends critically on the scattered light background present during those measurements, with an increasing background decreasing the signal-to-noise ratio of those measurements. An increasing background effectively reduces the aperture of the coronagraphic telescope, or conversely increases the required exposure time. The 1σ errors in the measurement of coronal intensity, electron density, velocity and magnetic field strength vary linearly with the signal-to-noise ratio of the observed coronal spectrum with different proportionality constants. General expressions are developed to describe the induced measurement errors in these physical quantities by a background, and specific conditions expected from the proposed 4-m Advanced Technology Solar Telescope are described.

Acknowledgements

The authors would like to acknowledge contributions from many in the solar physics community, especially members of the ATST Coronal Working Group including J. Kuhn, T. Rimmele, R. Hubbard, M. Aschwanden, and A. Winebarger.

References

- Aschwanden, M. and Benz, A. O.: 1988, *Astrophys. J.* **332**, 447.
Benz, A. O.: 1986, *Solar Phys.* **104**, 99.
Brosius, J. W., Landi, E., Cook, J. W., Newmark, J. S., Gopalswamy, N., and Lara, A.: 2002, *Astrophys. J.* **574**, 453.
Delannée, C., Koutchmy, S., Veselovsky, I. S., and Zhukov, A. N.: 1998, *Astron. Astrophys.* **329**, 1111.
Evans, J. W.: 1948, *JOSA* **38**, 1083.
Flower, D. R. and Pineau des Forêts, G.: 1973, *Astron. Astrophys.* **24**, 181.
Gudiksen, B. V. and Nordlund, A.: 2002, *Astrophys. J.* **572**, L113.
Guhathakurta, M., Fisher, R. R., and Altrock, R. C.: 1993, *Astrophys. J.* **414**, L145.
Harvey, J. W.: 1988, in J. Christensen-Dalsgaard and S. Frandsen (eds.), 'Advances in Helio- and Asteroseismology', *IAU Symp.* **123**, 497.
Judge, P. G., Hubeny, V., and Brown, J. C.: 1997, *Astrophys. J.* **475**, 275.
Judge, P. G., Casini, R., Tomczyk, S., Edwards, D. P., and Francis, E.: 2001, NCAR Technical Note, TN446, NCAR, Boulder.

- Judge, P. G., Tomczyk, S., Livingston, W. C., Keller, C. U., and Penn, M. J.: 2002, *Astrophys. J.* **576**, L157.
- Kuhn, J. R., MacQueen, R. M., Streete, J., Tansey, G., Mann, I., Hillebrand, P., Coulter R., Lin, H., Edmunds, D., and Judge, P.: 1999a, *Astrophys. J.* **521**, 478.
- Kuhn, J. R., Waterson, M., Northcott, M., Maberry, M., and Tokunaga, A.: 1999b, AMOS Technical Conference Maui Economic Development Board, Inc., Kahului, p. 85.
- Kuhn, J. R., Coulter, R., Lin, H., and Mickey, D. L.: 2003, *SPIE* **4853**, 318.
- Landi, E.: 2002, *Astron. Astrophys.* **382**, 1106.
- Lee, J., White, S. M., Kundu, M. R., Mikić, Z., and McClymont, A. N.: 1999, *Astrophys. J.* **510**, 413.
- Lin, H., Penn, M. J., and Tomczyk, S.: 2000, *Astrophys. J.* **541**, L83.
- McPherson, M. R., Lin, H. and Kuhn, J. R.: 1992, *Solar Phys.* **139**, 255.
- Melrose, D. B.: 1975, *Solar Phys.* **43**, 79.
- Mullan, D. J.: 1990, *Astron. Astrophys.* **232**, 520.
- Orrall, F. and Rottman, G.: 1986, in A. Poland (ed.), *NASA CP-2442 Coronal and Prominence Plasma*, p. 395.
- Parker, E. N.: 1988, *Astrophys. J.* **330**, 474.
- Penn, M. J. and Kuhn, J. R.: 1994a, *Astrophys. J.* **434**, 807.
- Penn, M. J. and Kuhn, J. R.: 1994b, *Solar Phys.* **151**, 51.
- Penn, M. J., Arnaud, J., Mickey, D. L., and LaBonte, B. J.: 1994, *Astrophys. J.* **436**, 368.
- Schrijver, C. J., Title, A. M., Berger, T. E., Fletcher, L., Hurlburt, N. E., Nightingale, R. W., Shine, R. A., Tarbell, T. D., Wolfson, J., Golub, L., Bookbinder, J. A., DeLuca, E. E., McMullen, R. A., Warren, H. P., Kankelborg, C. C., Handy, B. N., and De Pontieu, B.: 1999, *Solar Phys.* **187**, 261.
- Stockman, P., Bely, P., and Burrows, C.: 1996, *NGST Report: A Study of Optimum Mirror Configurations MSFC*, NASA.
- van de Hulst, H. C.: 1953, in G. P. Kuiper (ed.), *The Sun*, The University of Chicago Press, Chicago, p. 207.
- Vourlidas, A., Klimchuk, J. A., Korendyke, C. M., Tarbell, T. D., and Handy, B. N.: 2001, *Astrophys. J.* **563**, 374.
- Zhukov, A. N. Veselovsky, I. S., Koutchmy, S., and Delannee, C.: 2000, *Astron. Astrophys.* **353**, 786.